Available online at www.sciencedirect.com
ScienceDirect
Bioorganic & Medicinal Chemistry 16 (2008) 4313–4322
Bioorganic & Medicinal Chemistry

Potential antitumoral properties of a new copper complex with santonic acid

Patricia A. M. Williams,[a] Juan Zinczuk,[b] Daniel A. Barrio,[c] Oscar E. Piro,[d] Otaciro R. Nascimento[e] and Susana B. Etcheverry[a,c,*]

[a]*Centro de Química Inorgánica (CEQUINOR/CONICET, UNLP), Facultad de Ciencias Exactas, Universidad Nacional de La Plata, C. Correo 962, 1900 La Plata, Argentina*
[b]*Instituto de Química Orgánica de Síntesis (IQUIOS/CONICET, UNR), Facultad de Ciencias Bioquímicas y Farmacéuticas, Universidad Nacional de Rosario, 2000 Rosario, Argentina*
[c]*Cátedra de Bioquímica Patológica, Facultad de Ciencias Exactas, Universidad Nacional de La Plata, 47 y 115, 1900 La Plata, Argentina*
[d]*Departamento de Física, Facultad de Ciencias Exactas, Universidad Nacional de La Plata e Instituto IFLP (CONICET), C.C. 67, 1900 La Plata, Argentina*
[e]*Departamento de Física e Informática, Instituto de Física de São Carlos, Universidade de São Paulo-USP São Carlos, SP, Brazil*

Received 11 December 2007; revised 22 February 2008; accepted 25 February 2008
Available online 29 February 2008

Abstract—A new copper(II) complex of santonic acid $[Cu_2(sant)_4(H_2O)_2]\cdot 2\frac{1}{2}H_2O$ has been prepared and characterized by electronic, vibrational, EPR spectral studies, and stability determinations in solution. The presence of two antiferrromagnetically coupled copper centers in the solid state was detected by EPR. The dinuclear Cu(II) complex crystallizes in the tetragonal $P4_32_12$ space group, with $a = b = 14.498(3)$, $c = 64.07(1)$ Å. Biological studies indicate that the complex displays interesting potential antitumoral actions.

1. Introduction

Parasitic nematodes are among the most common and economically important infectious diseases of grazing livestock, especially in small ruminants. The development of safer ascaricides is the aim in the field of the veterinarian pharmacology against helmintic infections in the livestock. Synthetic anthelmintics, namely ivermectin, pyrantel, and piperazine have long been considered the most effective way of controlling parasitic infections. Because of the rapid escalation of anthelmintic resistance worldwide, other approaches to nematode control are developed. This has stimulated research into alternative medications, such as medicinal plants. Naturally produced plant anthelmintics offer possible alternatives that may be both sustainable and environmentally acceptable.[1,2] The active ingredients of the extracts of *Myrsinacaea* and *Artemisia* are embelin and santonin, respectively, which are chemically characterized. Sesquiterpenes are a class of naturally occurring molecules that have demonstrated therapeutic potential in decreasing the progression of cancer. These molecules are 15-carbon isoprenoid compounds that are typically found in plants and marine life. This class of compounds has frequently provided encouraging leads for chemotherapeutics, displaying potential as anticancer agents.[3] Santonic acid (Fig. 1) is derived from the sesquiterpenoid (−)-α-santonin, whose transformations have provided rich subject material for numerous structural, analytical, and synthetic studies.

As part of a project devoted to the development of transition metal complexes with potential pharmacological properties, the synthesis and structural characterization of the binuclear complex Cu(II)–santonic acid is reported. Furthermore, copper deficiency includes some skeletal alterations such as metaphyseal dysplasia, osteoporosis, and fracture of the long bones. Besides, it is well known that once absorbed many metal compounds

Keywords: Santonic acid copper; Osteoblast-like cells; Human colon adenocarcinoma cells.
* Corresponding author. Tel./fax: +54 0221 4259485; e-mail: etcheverry@biol.unlp.edu.ar

0968-0896/$ - see front matter © 2008 Elsevier Ltd. All rights reserved.
doi:10.1016/j.bmc.2008.02.075

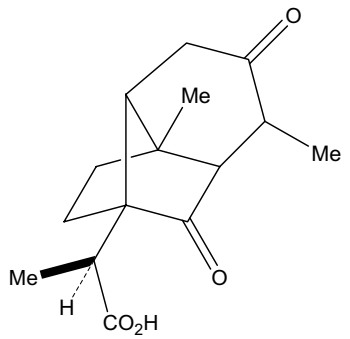

Figure 1. Scheme of santonic acid.

are distributed among tissues in the organisms and stored mainly in bone.[4–6] For this reason it is interesting to investigate the effects of the biometal, the organic active drugs and their metal complexes on bone-related cells. In the present study, the effect of these compounds has been tested on two osteoblast-like cells in culture, one normal (MC3T3E1) and the other tumoral (UMR106). In order to expand the study of the possible antitumoral properties of this complex, the effects were also tested on two human colon adenocarcinoma cell lines (Caco-2 and TC7).

2. Results and discussion

2.1. Structural results

Bond distances and angles around the metals in the complex are given in Table 1. An ORTEP[7] molecular plot of the Cu(II) dinuclear complex is shown in Figure 2.

Table 1. Bond lengths [Å] and angles [°] around copper in $[Cu_2(sant)_4(H_2O)_2]\cdot 2\frac{1}{2}H_2O$

Cu(1)–Cu(2)	2.606(3)	O(11)–Cu(1)–O(31)	168.2(6)
Cu(1)–O(11)	1.92(1)	O(11)–Cu(1)–O(41)	89.9(5)
Cu(1)–O(31)	1.95(1)	O(31)–Cu(1)–O(41)	88.1(5)
Cu(1)–O(41)	1.97(1)	O(11)–Cu(1)–O(21)	88.8(5)
Cu(1)–O(21)	1.97(1)	O(31)–Cu(1)–O(21)	90.2(5)
Cu(1)–O(1W)	2.16(1)	O(41)–Cu(1)–O(21)	165.6(7)
Cu(2)–O(12)	1.95(1)	O(11)-Cu(1)–O(1W)	92.8(6)
Cu(2)–O(22)	1.96(1)	O(31)-Cu(1)–O(1W)	98.8(6)
Cu(2)–O(42)	1.99(2)	O(41)-Cu(1)–O(1W)	91.4(6)
Cu(2)–O(32)	2.00(2)	O(21)–Cu(1)–O(1W)	103.0(6)
Cu(2)–O(2W)	2.26(1)	O(11)–Cu(1)–Cu(2)	83.2(4)
		O(31)–Cu(1)–Cu(2)	85.1(4)
		O(41)–Cu(1)–Cu(2)	82.0(5)
		O(21)–Cu(1)–Cu(2)	83.6(4)
		O(1W)–Cu(1)–Cu(2)	172.2(5)
		O(12)–Cu(2)–O(22)	87.7(6)
		O(12)–Cu(2)–O(42)	88.5(6)
		O(22)–Cu(2)–O(42)	168.7(6)
		O(12)–Cu(2)–O(32)	168.6(6)
		O(22)–Cu(2)–O(32)	90.7(6)
		O(42)–Cu(2)–O(32)	91.0(6)
		O(12)–Cu(2)–O(2W)	101.3(6)
		O(22)–Cu(2)–O(2W)	100.7(6)
		O(42)–Cu(2)–O(2W)	90.4(6)
		O(32)–Cu(2)–O(2W)	90.0(6)
		O(12)–Cu(2)–Cu(1)	85.2(4)

The dimeric complex exhibits a distorted lantern-like conformation, typical of dicopper carboxylate complexes (see, for example, Refs. 8 and 9). The pair of Cu(II) ions in a dimer is bridged through the carboxylic groups of four santoric molecules. Each copper ion is in an elongated octahedral environment, coordinated equatorially to four carboxylic oxygen atoms [Cu–O bond distances vary from 1.92(1) to 2.00(2) Å] and axially to a water molecule [Cu–Ow distances of 2.16(1) and 2.26(1) Å] and to the other Cu(II) ion, 2.606(3) Å apart. Opposite carboxylic groups are twisted with respect to each other in about 25°.

The conformation of the four santonic ligands closely resembles to one another and to the native santonic acid.[10] In fact, the ligands' common molecular frameworks can be least-squares fitted to one another by the Kabsh's procedure[11] giving a rms deviation of homologous atoms that varies from 0.105 to 0.197 Å. The best least-squares superposition of these ligands to the santonic acid leads to corresponding rms values in the range from 0.108 to 0.158 Å.

Ligands #1, 3, and 4 show asymmetric Cu...O=C–O...Cu bridging where longer Cu...O distances [in the range from 1.96(1) to 2.00(2) Å] correlates with adjacent carboxylic O=C double bonds [lengths from 1.20(2) to 1.28(2) Å] while shorter O...Cu distances [from 1.91(1) to 1.97(1) Å] correspond to adjacent C–O single bonds [lengths from 1.28(2) to 1.33(2) Å]. Ligand #2 Cu...O–C–O...Cu bridging is more symmetric [Cu...O distances of 1.95(1) and 1.97(1) Å] and therefore the carboxylic group shows a more delocalized bonding structure [C–O bond distances of 1.23(2) and 1.25(2) Å].

There are three crystallization water molecules, one of them sited at a crystallographic twofold axis. The short Ow...Ow and Ow...O(ket) distances [in the range from 2.67 to 3.281 Å] and corresponding Cu...Ow...Ow, Cu...Ow...O(ket), Ow...Ow...Ow, and Ow...Ow...O(ket) angles [from 100° to 140°] suggest an extended H-bonding network in the lattice.

2.2. Electronic spectrum

The electronic spectra of dinuclear carboxylate copper(II) complexes usually show two transitions (Bands I and II). Band I has been identified as copper(II) d → d transitions. This band, due to the $d_{xz,yz} \rightarrow d_{x^2-y^2}$ transition is broad and presents a shoulder at lower energies corresponding to the $d_z^2 \rightarrow d_{x^2-y^2}$ transition. Band II, traditionally assigned to Cu–Cu transitions has been recently considered indicative of a charge transfer transition between carboxylic oxygens and the metal ion and is characteristic of bridged systems with antiferromagnetic interactions.[12–14] The diffuse reflectance spectrum of the solid powder displays a broad Band I centered at 690 nm and a band (Band II) located at 390 nm. These bands shift at 704 nm ($\varepsilon = 190\ M^{-1}\ cm^{-1}$) and 380 nm ($\varepsilon = 350\ M^{-1}\ cm^{-1}$) in the UV–vis spectrum of an ethanolic solution of the complex. The position of Band I indicates an oxygenated environment around de copper ion and the epsilon

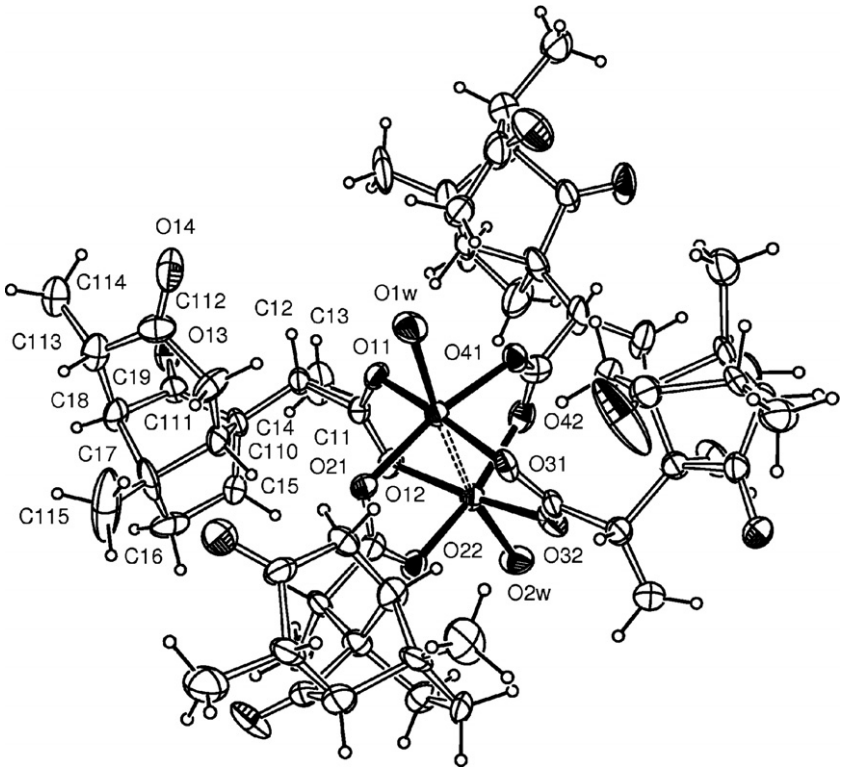

Figure 2. Molecular plot of the copper(II) dinuclear complex in $[Cu_2(sant)_4(H_2O)_2]\cdot 2\frac{1}{2}H_2O$ showing the labeling scheme of the non-H atoms and their displacement ellipsoids at the 20% probability level. Copper–oxygen bonds are indicated by solid lines and Cu...Cu contact by dashed line. For clarity, only one santonic ligand has been fully labeled.

value suggests a tetragonal distortion of the coordination sphere. The higher intensity of Band II implies a charge transfer transition.[13]

2.3. Stability studies

Due to the linearity of the plot of $\ln A$ (A = absorbance at 380 nm) versus time, the decomposition of $[Cu_2(sant)_4(H_2O)_2]\cdot 2\frac{1}{2}H_2O$ (CuSant) is demonstrated to be of the first order in the concentrations of the complex. The decomposition rate of the complex was determined in ethanol at 25 °C since the stock solutions for EPR and UV–vis determinations were prepared in this solvent at room temperature. The rate constant for the decomposition of the dimer into monomers of a 0.15 mM CuSant solution was $k = 3.66 \times 10^{-3}\ \text{min}^{-1}$. The presence of monomeric impurities in the EPR spectrum (see below) can be assigned to the split of the bridge between the two copper centers, rendering near 2% of the monomer during the manipulation time.

2.4. Vibrational spectroscopy

As it can be seen from Table 2 the band corresponding to the carboxylic acid stretching (νC=O) splits into two new strong bands assigned to the symmetric and antisymmetric vibrations of the deprotonated carboxylate groups coordinated to the copper cation. The value of the difference between these two absorption bands together with the results of structural data, UV–vis spectrum and EPR determinations (see below) indicates that the carboxylate anion binds to two copper centers in a bridging mode.[9,15] The band at 1731 cm^{-1} has been assigned to the C=O stretching of the 'strained' γ-ketone. The ε-ketone band is masked by the C=O stretching of the carboxylic acid (1683 cm^{-1}). Upon deprotonation of the carboxylic acid group and coordination with the metal ions, the characteristic C=O stretching band of the carboxylic acid disappeared and this change allowed the observation of ν(C=O), ε-ketone at 1706 cm^{-1}, as it has been previously reported.[16,17]

Moreover in the copper complex the O–H stretching band of the coordinated water molecules appeared as a broad band at 3500 cm^{-1}. The bending modes of these groups are overlapped with the strong bands located at ca. 1600 cm^{-1}.

Table 2. Assignment of the main bands of the infrared spectra of santonic acid (Hsant), and the copper complex (CuSant) (band positions in cm^{-1})

HSant	CuSant	Assignments
	3500^{br}	ν(O–H)
1731^{vs}	1736^{vs}	ν(C=O), γ-ketone, strained
	1706^{vs}	ν(C=O), ε-ketone
1683^{s}		ν(C=O), carboxylic acid and ν(C=O), ε-ketone
	1617^{vs}	$\nu_{as}(COO^-)$
	1415^{vs}	$\nu_{s}(COO^-)$
1182^{s}		ν(C–O), carboxylic acid

vs, very strong; s, strong; br, broad.

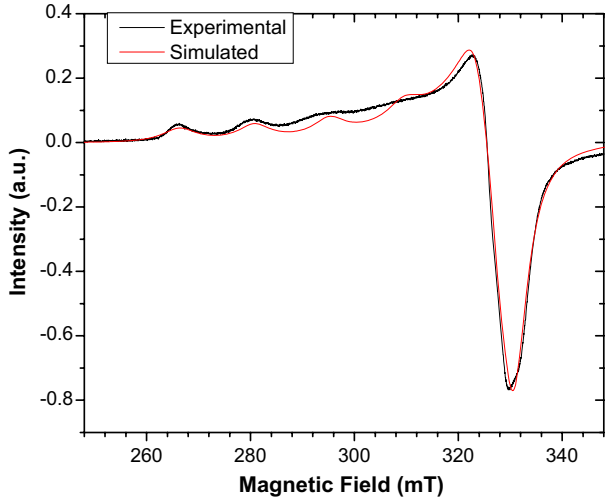

Figure 3. EPR spectrum of $[Cu_2(sant)_4(H_2O)_2]\cdot 2\frac{1}{2}H_2O$ in ethanol at 4.3 K (——) experimental and (——) simulated. Frequency = 9.480 GHz. *Q*-Values: 22.0 and 9.0 MHz. Lorentzian shape.

2.5. EPR spectra

The presence of strong antiferromagnetic interaction in the solid dinuclear complex has been determined by the absence of the X-band EPR signal at liquid helium temperature. Usually, dinuclear copper complexes present this type of coupling (S=0) at 4 K.[18,19] The $\Delta Ms = \pm 2$ transitions at half field were not observed. This is probable due to long-range inter-dimeric magnetic coupling between the dimer upper level $S = 1$ spins of neighboring dinuclear complexes. The corresponding super-exchange interactions could be in part mediated by the presumed H-bond network described in Section 2.1.

The solution EPR spectrum recorded in ethanol at 4.3 K shows a very weak EPR signal attributed to a small amount of a monomeric impurity of the dissolved complex. The spectrum is characteristic of an axial symmetry with ($g_{II} > g_{\perp}$). This indicates that the unpaired electron is located mostly on $d_{x^2-y^2}$ orbital of the copper(II) atom. The experimental and simulated spectra are shown in Figure 3. Simulation has shown that the molecule has axial symmetry with *g*: 2.0700 (g_x), 2.0790 (g_y), 2.3525 (g_z) typical of a square pyramidal environment of copper(II) complexes. The hyperfine coupling constant components, $A(x) = A(y) = 10 \times 10^{-4}\,cm^{-1}$ *y* $A(z) = 155 \times 10^{-4}\,cm^{-1}$ point to an oxygenated coordination sphere around the metal center.[20]

2.6. Cell proliferation

Previous to the proliferation studies with the copper compounds the effect of DMSO 0.5%–serum-free DMEM (Dulbecco's modified Eagle's medium) 99.5% was tested in order to determine any toxic effect attributed to DMSO. At this maximum concentration used for the organic solvent no effect was observed on cell survival. The effects of the hexaacuocopper(II) ion and the complex can be observed in Figures 4 and 5.

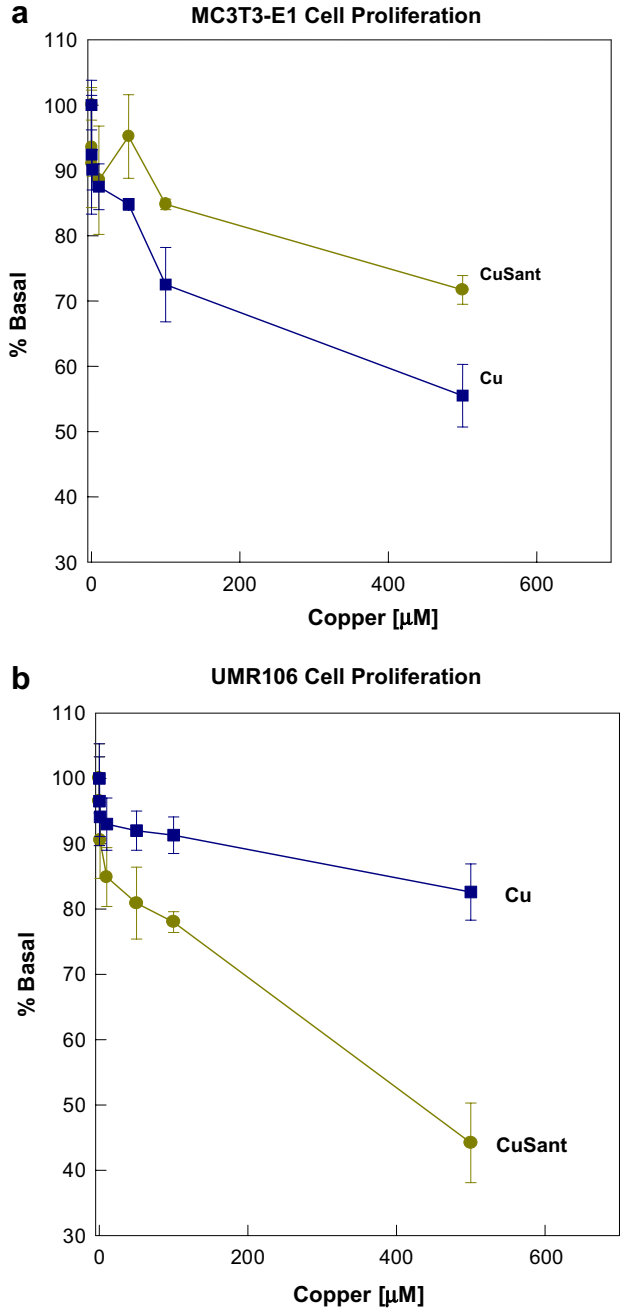

Figure 4. Effect of copper(II) (■) and $[Cu_2(sant)_4(H_2O)_2]\cdot 2\frac{1}{2}H_2O$ (●) compounds on MC3T3E1 (a) and UMR106 (b) cell proliferation. Cells were incubated in serum-free DMEM alone (basal) or with different concentrations of free copper (from $CuCl_2$) and the complex CuSant (per copper atom) at 37 °C for 24 h. Results are expressed as % basal and represent means ± SEM, of three independent experiments carried out in triplicate.

Besides, santonic acid did not cause any significant effect on cell proliferation of all the cell lines employed in this study in the whole range of concentration (data not shown). The copper complex in a copper concentration of 500 µM produced a stronger inhibition (55% of basal) on tumoral osteoblasts (UMR106) than on the non-transformed cells (25% of basal) (MC3T3E1) (Fig. 4a and b).

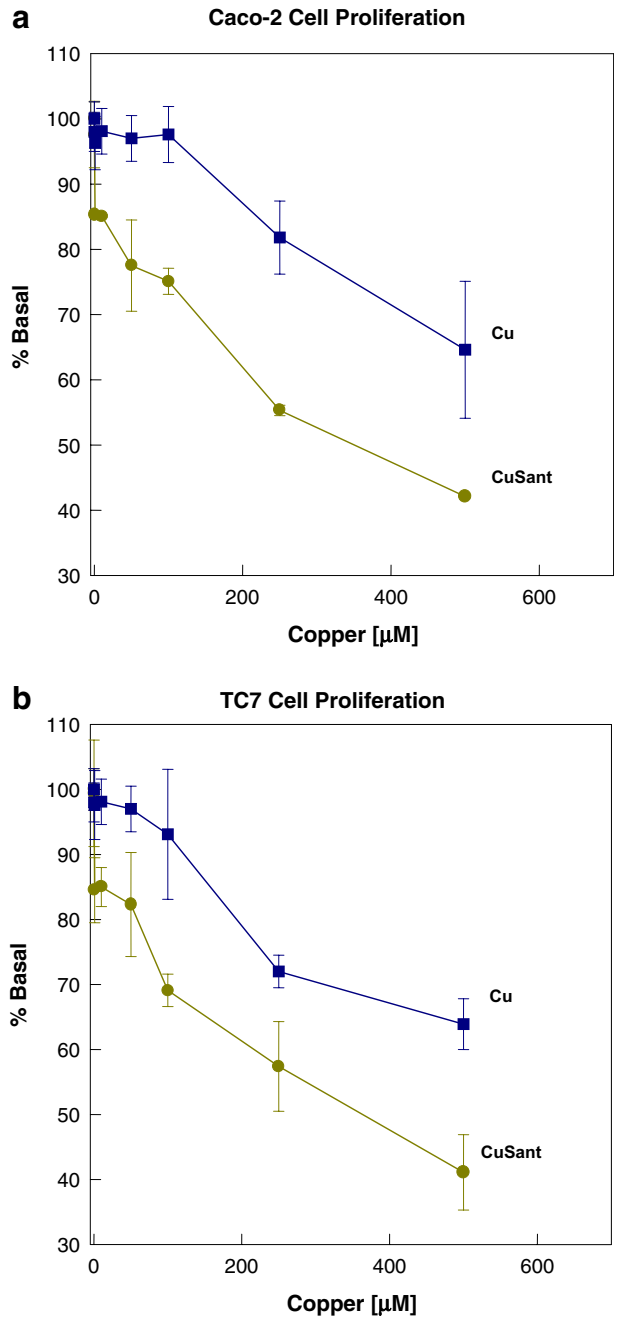

Figure 5. Effect of $CuCl_2$ (■) and $[Cu_2(sant)_4(H_2O)_2]\cdot 2\frac{1}{2}H_2O$ (●) compounds on Caco-2 (a) and TC7 (b) cell proliferation. The experimental conditions were similar to those of Figure 3. Results are expressed as % basal and represent means ± SEM, of three independent experiments carried out in triplicate.

Hexaacuocopper(II) produced a stronger decrease in cell proliferation (45% of basal, 500 μM) than the complexed copper (CuSant) on the normal osteoblasts in culture. On the contrary, it did not exert any significant effect on the tumoral ostoeblasts up to 500 μM. In the human colon adenocarcinoma cell lines CuSant exerted stronger inhibition on cell proliferation than the free copper ion (Fig. 5a and b). The inhibition of the 500 μM complex reached a value of ca. 55–60% of the basal value for the three tested tumoral lines. Taking into consideration the high antiproliferative effect of the complex in tumoral cell lines, it may be considered as a potential candidate for future antineoplastic studies.

2.7. Cell morphology

The ability of CuSant, free copper ions and santonic acid to induce morphological changes was investigated in the four cultured cell lines. After overnight incubation in a serum-free medium with or without the addition of the compounds, cells were fixed, stained, and observed by light microscopy. Under these starved conditions, a moderate number of cells started to detach from the culture dishes.

In the case of MC3T3E1 cells (Fig. 6a) the monolayer of the control showed the aspect of a typical fibroblast-like culture. Cells were stellate in shape and exhibited slender lamellar expansions. These processes appeared to connect each other among neighbor cells. The nuclei contained moderately thick chromatin granules, while the cytoplasm showed numerous inclusions and vacuoles. After treating the culture with 500 μM hexaacuocopper(II) ions, the cytoplasms are denser and thinner and the cells become more fusiform. The nuclei retain their normal characteristics (Fig. 6b). Incubation of the cells with 500 μM CuSant caused the following changes: the cells become more elongated than when treated with $[Cu(H_2O)_6]^{2+}$ alone. The nuclei also acquire fusiform shape. As in the case of copper addition there are a few number of cells by field (see Fig. 6c).

For UMR106 cells the control (medium alone) showed a polygonal morphology with irregular nuclei that showed great amount of nucleoles. Cells displayed abundant intercellular connections (Fig. 7a). When incubated with $[Cu(H_2O)_6]^{2+}$ ion, few cells by field with trapezoidal form and few and very long intercellular connections were observed. The nuclei were condensed with vacuoles in their interior. It was not possible to distinguish the nucleoles (Fig. 7b). The complex produced a similar effect to copper(II) ions but a smaller number of cells by field can be observed in this case. The cells display a neuron-like shape (Fig. 7c).

The characteristics of Caco-2 cells can be seen in Figure 8. The cells displayed polygonal form with great nuclei with numerous nucleoles. Several intercellular connections are observed (Fig. 8a).[21] Upon incubation with copper(II) ions, the cytoplasmic borders became weakly visible. In the cytoplasm numerous irregular vacuoles were observed. The nuclei are condensed without visible nucleoles (Fig. 8b). The previously described effects for the treatment with $[Cu(H_2O)_6]^{2+}$ appeared more noticeable with the addition of the complex. The nuclei were more condensed and irregular. There were abundant irregular vacuoles in the cytoplasmic region. Smaller number of cells by field could be seen in agreement with the results of the cellular proliferation (Fig. 8c).

The morphological changes induced in TC7 cells, a subclone of Caco-2 cells, were the same as those displayed

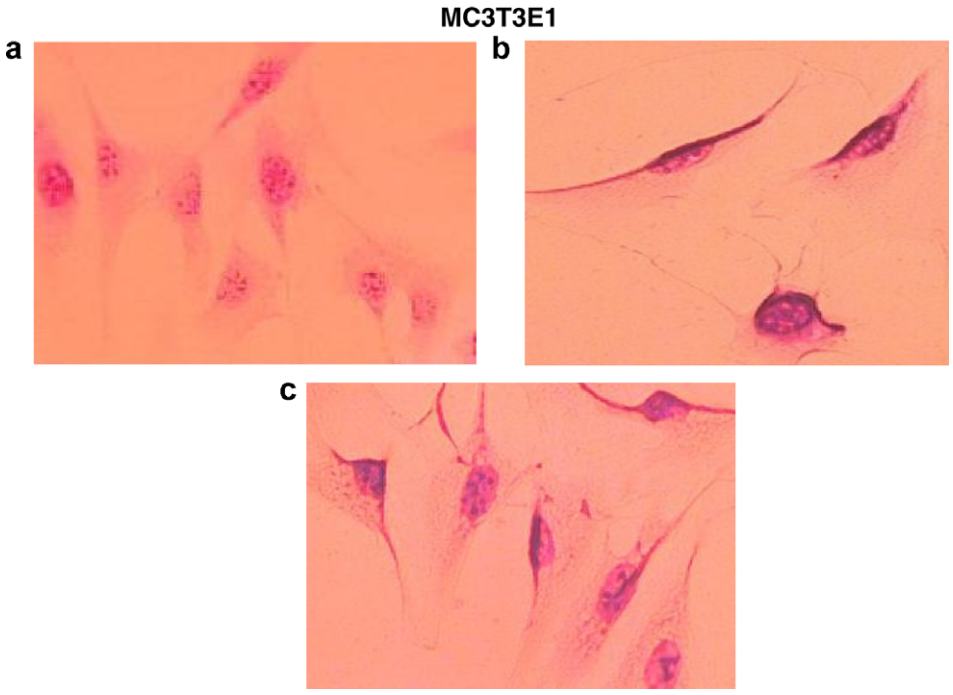

Figure 6. Effect on cell morphology for the treatment of the osteoblast-like cells MC3T3E1 without drug addition (control) (a) with $CuCl_2$ (500 μM) (b), and $[Cu_2(sant)_4(H_2O)_2]\cdot 2\frac{1}{2}H_2O$ (500 μM per copper atom) (c). (objective 40×).

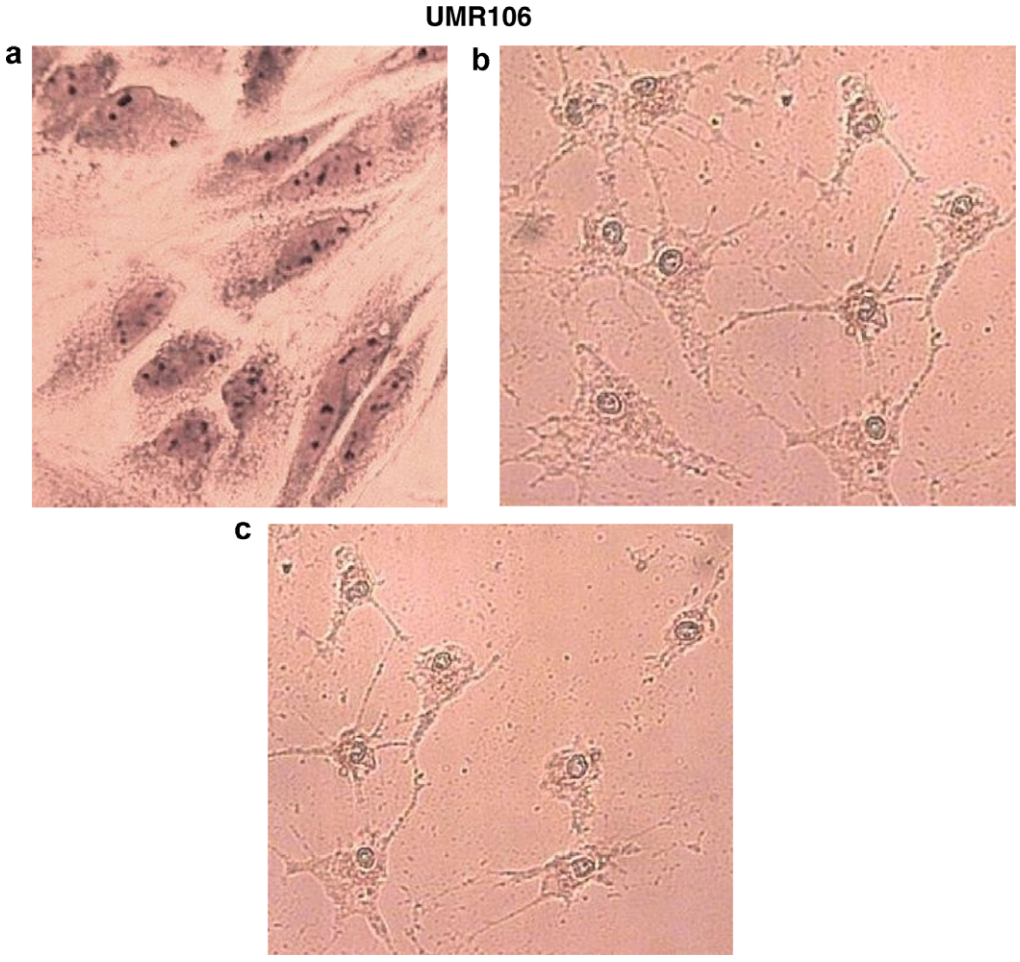

Figure 7. Effect on cell morphology for the treatment of the osteosarcoma UMR106 cells without drug addition (control) (a) with copper (500 μM $CuCl_2$) (b), and $[Cu_2(sant)_4(H_2O)_2]\cdot 2\frac{1}{2}H_2O$ (500 μM per copper atom) (c). (objective 40×).

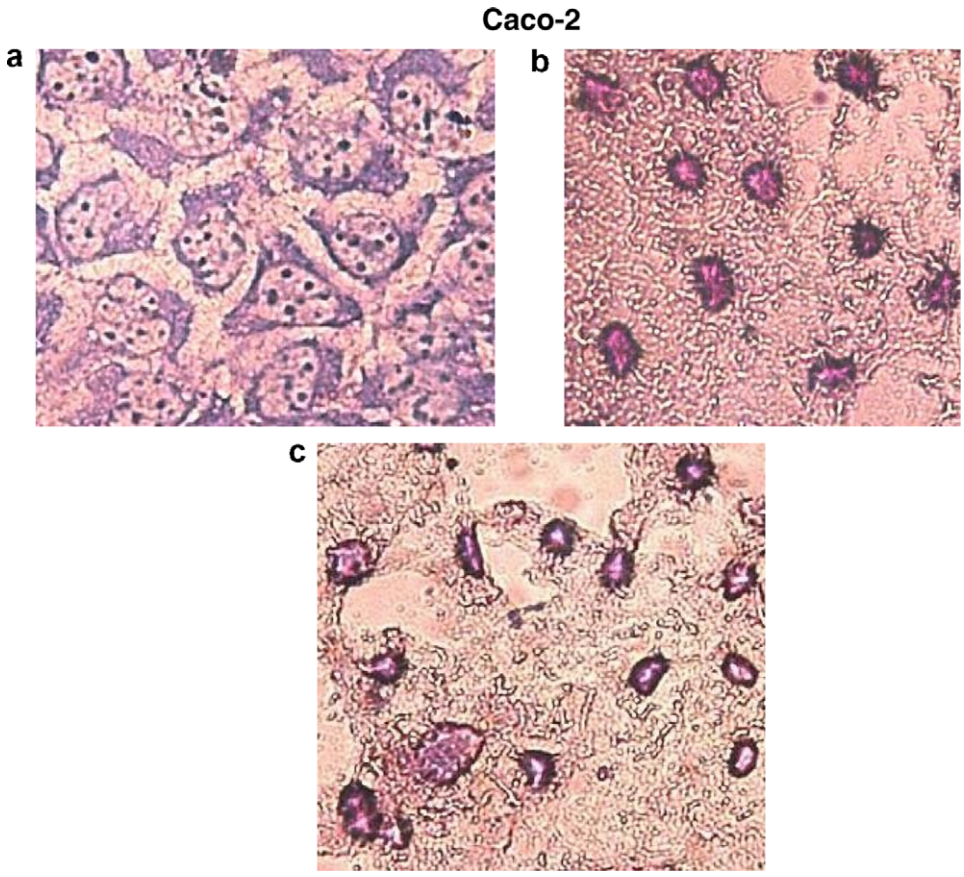

Figure 8. Effect on cell morphology for the treatment of the human colon adenocarcinoma Caco-2 cells without drug addition (control) (a) with copper (500 μM $CuCl_2$) (b), and $[Cu_2(sant)_4(H_2O)_2]\cdot 2\frac{1}{2}H_2O$ (500 μM per copper atom) (c). (objective 40×).

by Caco-2 (data not shown). Santonic acid did not induce any morphological change in the four cell lines.

3. Conclusions

The present study reveals the potential antitumoral activity of the complex $[Cu_2(sant)_4(H_2O)_2]\cdot 2\frac{1}{2}H_2O$ obtained and characterized for the first time. The dimeric structure of the complex has been established by crystallographic data. The lack of EPR signals in the solid state supported that there exists a strong antiferromagnetic coupling between the two metallic nuclei. The infrared and the diffuse reflectance spectral determinations also confirmed the carboxylate bridges between two Cu(II) ions.

The bioactivity of the new complex was tested in four cell lines in culture. For the osteoblastic-like cells the complexation of copper with santonic acid modulated the toxic effect of the free ion. In the normal osteoblasts the complex caused a significantly smaller inhibition than copper(II) while in the tumoral osteosarcoma cells the complex was more deleterious. The stronger inhibition of the complex in the tumoral cells is promissory for further in vivo investigations of its antitumoral properties. This behavior correlated with the action of the complex in other two tumoral cell lines of human colon adenocarcinoma, where the inhibitory power of the complex was ca. 60% while the free metallic ion produced an inhibition of only 35%. Morphological cellular observations were in accord with proliferation studies since the greater alterations in the nuclei and cytoplasms were displayed by the complex treated cells. In these cases, the number of surviving cells per field was statistically lower than for control conditions. The cytotoxic properties of the new complex have been established in the three tumoral cell lines. Altogether these promising results point to the interest of the synthesis and characterization of new copper coordination compounds to be tested in different tumoral cell lines in order to establish their potential antitumoral properties.

4. Experimental

Santonic acid has been prepared according to Brunskill et al.[22] $CuCO_3\cdot Cu(OH)_2$ was synthesized according to reported methods.[23] Corning or Falcon provided tissue culture materials. DMEM and trypsin–EDTA were purchased from Gibco (Gaithersburg, MD, USA) and fetal bovine serum (FBS) from Gibco-BRL (Life Technologies, Germany). All other chemicals used were of analytical grade. The electronic UV–vis spectra were recorded on a Hewlett–Packard 8453 diode-array spectrophotometer. Diffuse reflectance spectrum was registered with a Shimadzu UV-300 instrument, using MgO as an internal standard. Infrared spectra were recorded on a Bruker IFS 66 FTIR-spectrophotometer from 4000 to 400 cm^{-1} using the KBr pellet technique. Elemental analysis for carbon and hydrogen was performed using

a Carlo Erba EA 1108 analyzer. Electron paramagnetic resonance spectra of the Cu(II) ion were recorded on a Bruker ELEXSYS E580 (Bruker BioSpin, Rheinstetten, Germany) at liquid helium temperatures (4 K). The temperature was controlled by an Oxford ITC503 cryogenic system. EPR samples were frozen by immersion in liquid nitrogen and then placed in the spectrometer cavity. The microwave frequency was 9.4752 GHz; modulation amplitude, 0.5 mT; modulation frequency, 100 kHz; microwave power 10.08 mW, and sweep field 120.0 mT. The Cu(II) EPR parameters were determined by means of spectral simulation using the Bruker WinEPR-SimFonia program.

4.1. Synthesis of the complex

A solution of santonic acid (1 mmol, 264 mg) in methyl alcohol (10 mL) is warmed at 50 °C. The solution is added to a suspension of $CuCO_3{\cdot}Cu(OH)_2$ (0.75 mmol, 166 mg) in water (25 mL) and stirred for 30 min with heating. The green powder obtained is filtered and washed with methyl alcohol. Green monocrystals suitable for X-ray structure determinations are obtained by recrystallization from ethyl alcohol in 5 days. Anal. Calcd $C_{60}H_{85}O_{20.5}Cu_2$: C, 57.1; H, 6.7. Exp: C, 57.2; H, 6.6. Yield: 81%.

4.2. Diffraction data and structure solution and refinement

Crystal data, structure solution methods, and refinement results are summarized in Table 3.[24–28] The crystal diffracted poorly; in fact, only about 61% of the reflection intensities up to 0.85 Å resolution were above two standard deviations of measurement errors. This leads to a low reflection to parameter ratio and consequently to rather limited crystallographic agreement factors and bond distance and angle errors. The H-atoms of the santonic ligand groups were positioned stereochemically and refined with the riding model. The methyl hydrogen atom locations were optimized during the refinement by treating them as rigid bodies which were allowed to rotate around the corresponding C–C bond. The water hydrogen atoms could not be located in different Fourier maps and hence they were not included in the final molecular model.

Table 3. Crystal data and structure refinement for $[Cu_2(sant)_4(H_2O)_2]{\cdot}2\frac{1}{2}H_2O$ (CuSant)

Empirical formula	$C_{60}H_{81}Cu_2O_{20.5}$
Formula weight	1261.36
Temperature	296(2) K
Wavelength	1.54184 Å
Crystal system, space group	Tetragonal, $P4_32_12$ (#96)
Unit cell dimensions[a]	$a = b = 14.498(3)$ Å $c = 64.07(1)$ Å
Volume	13467(4) Å^3
Z, Calculated density	8, 1.244 mg/m^3
Absorption coefficient	1.344 mm^{-1}
$F(000)$	5336
Crystal color/shape	Blue/prism
Crystal size	$0.40 \times 0.32 \times 0.28$ mm
Diffractometer/scan	Enraf-Nonius CAD-4/ω-2ϑ
Radiation, graphite monochr.	CuKα, $\lambda = 1.54184$ Å
Scan width	$0.8 + 0.35 \tan\vartheta$
Standard reflection	(2, 8, −2)
ϑ range for data collection	2.76–65.13°
Index ranges	$0 \leqslant h \leqslant 12$, $0 \leqslant k \leqslant 16$, $-75 \leqslant l \leqslant 1$
Reflections collected/unique	6535/6509 [R(int) = 0.0154]
Observed reflections [$I > 2\sigma$(I)]	4251
Completeness to $\vartheta = 65.13°$	96.8%
Max. and min. transmission	0.726 and 0.667
Data collection	EXPRESS[24]
Data reduction and correction[b]	XCAD-4[25]
Absorption correction	PLATON[26]
Structure solution[c]	SHELXS-97[27]
Refinement[d]	SHELXL-97[28]
Refinement method	Full-matrix least-squares on F^2
Weights, w	$w = [\sigma^2(F_o^2) + (0.2P)^2]^{-1}$ $P = [\mathrm{Max}(F_o^2, 0) + 2F_c^2]/3$
Data/restraints/parameters	6509/0/757
Goodness-of-fit on F^2	1.933
Final R indices[e] [$I > 2\sigma(I)$]	$R_1 = 0.1558$, $wR_2 = 0.4105$
R indices (all data)	$R_1 = 0.2108$, $wR_2 = 0.4678$
Absolute structure parameter	0.29(15)
Extinction coefficient	0.0008(2)
Largest different peak and hole	1.380 and −0.966 e A^{-3}

[a] Least-squares refinement of $[(\sin\vartheta)/\lambda]^2$ values for 24 reflections in the $17.44 < \vartheta < 33.03°$ range.
[b] Lorentz and polarization corrections.
[c] Structure solved by direct and Fourier methods.
[d] Neutral scattering factors and anomalous dispersion corrections. Final molecular model obtained by anisotropic full-matrix least-squares refinement of non-hydrogen atoms.
[e] R indices defined as: $RI = \Sigma||F_o| - |F_c||/\Sigma|F_o|$, $wR_2 = [\Sigma w(F_o^2 - F_c^2)^2/\Sigma w(F_o^2)^2]^{1/2}$.

4.3. Stability studies

To test the stability of the ethanolic solutions of CuSant used in the UV–vis and EPR spectra, we analyzed the electronic spectra recorded at times ranging from 0 to 5 h, at 25 °C. The rate of decomposition of the dimeric complex was spectrophotometrically measured at 380 nm (this band identified the dimeric structure of the complex, see below). The decomposition rate constant was estimated.

4.4. Cell culture

Rat osteosarcoma UMR106, osteoblastic non-transformed mouse calvaria-derived MC3T3E1 cells, human colon adenocarcinoma cell lines Caco-2, and TC7 were grown in DMEM supplemented with 10% (v/v) FBS and antibiotics (100 U/mL penicillin and 100 mg/mL streptomycin) in a humidified atmosphere of 95% air/5% CO_2. Cells were grown at near-confluence (70–80%) and were subcultured using 0.1% trypsin–1 mM EDTA in Ca^{2+}–Mg^{2+}-free phosphate-buffered saline (PBS). For experiments, 5.5×10^4 cells/well (UMR 106), 3.3×10^4 cells/well (MC3T3E1), and 1×10^5 cells/well, for Caco-2 and TC7 were plated into 24 well/plates. After the culture reached 70–80% confluence, the cells were washed twice with DMEM.

4.5. Cell proliferation assay

A mitogenic bioassay was carried out as described by Okajima et al. with some modifications.[29] Briefly, cells

in 24 well/plates were washed with PBS and fixed with 5% glutaraldehyde/PBS at room temperature for 10 min. Cells were then stained with 0.5% crystal violet/25% methanol for 10 min. After that, the dye solution was discarded and the plate was washed with water and dried. The dye in the cells was extracted using 0.5 mL/well 0.1 M glycine/HCl buffer, pH 3.0/30% methanol and transferred to test tubes. Absorbance was read at 540 nm after a convenient sample dilution. The correlation between cell number/well and the absorbance at 540 nm of diluted extraction sample after crystal violet staining has been previously established.[30] Data are expressed as means ± SEM. Statistical differences were analyzed using Student's *t*-test. *t*-Tests were done to compare treated cultures with the untreated cultures. Freshly prepared solutions of santonic acid, $CuCl_2$ and CuSant were added to the culture dishes at the following concentrations: 0, 5, 10, 25, 50, 100, and 500 μM. The dissolution of the complex was performed using DMSO 0.5% and serum-free DMEM 99.5% was added for the different concentrations. Considering the dimeric nature of the complex the final concentrations of the complex have been calculated per copper atom. The biological effects of these solutions were compared with those of free copper (from $CuCl_2$). Cells were incubated overnight with the compounds at different doses in serum-free DMEM.

4.6. Cell morphology

All the cell lines were grown in six well/plates. The cells were incubated overnight with fresh serum-free DMEM plus 0 (basal), 500 μM solutions of copper complex and Cu^{2+} ($CuCl_2$). The monolayers were subsequently washed twice with PBS, fixed with methanol, and stained with 1:10 dilution of Giemsa for 10 min.[31] Next, the monolayers were washed with water and the morphological changes were examined by light microscopy.

Acknowledgments

This work was supported by UNLP, CONICET, CICPBA, ANPCyT (PICT 10968, PIP 6366) and O.E.P., D.A.B., J.Z., and S.B.E. are members of the Carrera del Investigador, CONICET. P.A.M.W. is a member of the Carrera del Investigador CICPBA, Argentina. The X-ray diffraction experiments were carried out at LANADI (CONICET-UNLP).

Supplementary data

Listings of atomic fractional coordinates (Table S3), full bond distances and angles (Table S4), anisotropic displacement parameters (Table S5), positions of the hydrogen atom and their isotropic displacement parameters (Table S6), and presumed H-bond distances and angles (Table S7). Crystallographic data (without structure factors) for the structure reported in this paper have been deposited with the Cambridge Crystallographic Data Centre as supplementary publication No. CCDC 659505; e-mail: deposit@ccdc.cam.ac.uk; website: www.ccdc.cam.ac.uk.

Supplementary data associated with this article can be found, in the online version, at doi:10.1016/j.bmc.2008.02.075.

References and notes

1. Githiori, J. B.; Höglund, J.; Waller, P. J.; Leyden Baker, R. *Vet. Parasitol.* **2003**, *116*, 23.
2. Githiori, J. B.; Höglund, J.; Waller, P. J.; Leyden Baker, R. *Vet. Parasitol.* **2003**, *118*, 215.
3. Modzelewska, A.; Sur, S.; Kumar, S. K.; Khan, S. R. *Curr. Med. Chem. Anticancer Agents* **2005**, *5*, 477.
4. Lai, Y. L.; Yamaguchi, M. *Biol. Pharm. Bull.* **2005**, *28*, 2296.
5. Ytrehus, B.; Skagemo, H.; Stuve, G.; Sivertsen, T.; Handeland, K.; Vikøren, T. *J. Wildl. Dis.* **1999**, *35*, 204.
6. Ott, E. A.; Asquith, R. L. *J. Anim. Sci.* **1995**, *73*, 466.
7. Jonson, C. K. *ORTEP-II. A Fortran Thermal-Ellipsoid Plot Program. Report ORNL-5318*, Oak Ridge National Laboratory, Tennessee, USA, 1976.
8. Mehrotra, R. C.; Bohra, R. In *Metal Carboxylates*; Academic Press: London, 1983.
9. Kögerler, P.; Williams, P. A. M.; Parajón-Costa, B. S.; Baran, E. J.; Lezama, L.; Rojo, T.; Müller, A. *Inorg. Chim. Acta* **1998**, *268*, 239.
10. Brunskill, A. P. J.; Thompson, H. W.; Lalancette, R. A. *Acta Cryst.* **1999**, *C55*, 566.
11. Kabsch, W. *Acta Cryst.* **1976**, *A32*, 922.
12. Meier, J. L.; Coughenour, C. E.; Carlisle, J. A.; Carlisle, G. O. *Inorg. Chim. Acta* **1985**, *106*, 159.
13. Lever, A. B. P. In *Inorganic Electronic Spectroscopy*, 2nd ed.; Elsevier: Amsterdam, 1984.
14. Christidis, P. C.; Rentzeperis, P. J.; Sigalas, M. P.; Hadjikostas, C. C. *Z. Krystallogr.* **1986**, *176*, 103.
15. Latif, A. *J. Inorg. Biochem.* **1997**, *68*, 167.
16. Brunskill, A. P. J.; Thompson, H. W.; Lalancetre, R. A. *Acta Cryst.* **1999**, *C55*, 566.
17. Zinczuk, J.; Ruveda, E. A.; Thompson, H. W.; Lalancette, R. A. *Acta Cryst.* **2004**, *C60*, o408.
18. Rentschler, E.; Gatteschi, D.; Cornia, A.; Fabretti, A. C.; Barra, A.; Shchegolikhina, O. I.; Zhdanov, A. A. *Inorg. Chem.* **1996**, *35*, 4427.
19. Kannappan, R.; Mahalakshmy, R.; Rajendiran, T. M.; Venkatesan, R.; Sambasiva Rao, P. *Proc. Indian Acad. Sci. (Chem. Sci.)* **2003**, *115*, 1.
20. Hathaway, B. J.; Billing, D. E. *Coord. Chem. Rev.* **1970**, *5*, 143.
21. Walter, E.; Kissel, T. *Eur. J. Pharm Sci.* **1995**, *3*, 215.
22. Brunskill, A. P. J.; Thompson, H. W.; Lalancette, R. A. *Acta Cryst.* **1999**, *C55*, 566.
23. Brauer, G. In *Química Inorgánica Preparativa*, Reverté, Ed.; Barcelona, 1958.
24. Enraf-Nonius, D. *CAD4 Express Software*, The Netherlands, 1994.
25. Harms, K.; Wocadlo, S. *XCAD-4. Program for Processing CAD-4 Diffractometer Data*; University of Marburg: Marburg, Germany, 1995.
26. Spek, A. L. *PLATON, A Multipurpose Crystallographic Tool*; Utrecht University: Utrecht, The Netherlands, 1998.
27. Sheldrick, G. M. *SHELXS-97. Program for Crystal Structure Resolution*; University of Göttingen, Göttingen: Germany, 1997.

28. Sheldrick, G. M. *SHELXL-97. Program for Crystal Structures Analysis*; University of Göttingen: Göttingen, Germany, 1997.
29. Okajima, T.; Nakamura, K.; Zhang, H.; Ling, N.; Tanabe, T.; Yasuda, T.; Rozenfeld, R. G. *Endocrinology* **1992**, *130*, 2201.
30. Cortizo, A. M.; Etcheverry, S. B. *Mol. Cell. Biochem.* **1995**, *145*, 97.
31. Sálice, V. C.; Cortizo, A. M.; Gómez Dumm, C. L.; Etcheverry, S. B. *Mol. Cell. Biochem.* **1999**, *198*, 119.